Beyond Single Hazard Framework: Multi-Hazard Worst Case Scenarios from Ensemble Tropical Cyclone Forecasts

Md. Rezuanul Islam,[a] Tsutao Oizumi,[b] Le Duc,[a,b], Takuma Ota,[b] Takuya Kawabata[b], Yohei Sawada,[a]

[a] *Department of Civil Engineering, Graduate School of Engineering, the University of Tokyo, Tokyo, Japan*

[b] *Meteorological Research Institute, Tsukuba, Japan*

Corresponding author: Md. Rezuanul Islam, fahiemislam@gmail.com

ABSTRACT

Ensemble forecasting is a powerful tool for supporting informed decision-making in managing multi-hazard risks associated with tropical cyclones (TCs). Although TC ensemble forecasts are widely used in operational numerical weather prediction systems, their potential for disaster prediction and management has not been fully exploited. Here we propose a novel, efficient, and practical method to extract meaningful Multi-Hazard Worst Case Scenarios (MHWCS) from a large ensemble TC forecast of 1000-members. We performed the ensemble atmospheric forecasting of TC Hagibis (2019) using the Japan Meteorological Agency's (JMA) nonhydrostatic model. The simulated atmospheric predictions were serving as inputs for the JMA's operational flood forecast model, as well as statistical storm surge and gust wind models. These models estimate river flooding, storm surge, and wind hazard intensities in Tokyo. By accounting for uncertainties in ensemble multi-hazard forecasts, we objectively demonstrate that Pareto-optimal solutions can effectively identify the meaningful MHWCS. These solutions illustrate complex trade-offs among competing hazard components across various forecast locations. While some identified MHWCS pose severe risks for a single hazard type or location, others present moderately high risks across multiple hazards and locations. This diversity in potential scenarios requires risk managers to prepare multiple response strategies for both imminent risks and post-disaster management. Our findings further underscore the importance of evaluating Pareto-optimal solutions to assist forecasters and risk managers in understanding how combinations of TC meteorological variables—such as track, translation speed, size, intensity, and rainfall—shape worst-case scenarios.

SIGNIFICANCE STATEMENT

This work aims to maximize the benefits of ensemble tropical cyclone (TC) forecasts by introducing a novel multi-hazard worst case scenarios (MHWCS) framework. By examining a large ensemble forecast of river flooding, storm surge, and gust wind hazards due to TC Hagibis (2019) in Tokyo, this approach objectively identifies, for the first time, MHWCS that maximize multi-hazard intensities relative to the ensemble mean, implying no other ensemble members offer better representations. Identifying this sub-set of ensemble forecasts, which reflects complex interdependencies between hazards, is crucial for better preparing and protecting communities. The study highlights how evaluating forecast meteorological variables of MHWCS can help forecasters and decision makers better understand TC characteristics that trigger significant multi-hazard impacts.

1. Introduction

Tropical cyclones (TCs) serve as classic examples of multi-hazards, where several hazard drivers—such as wind, storm surge, and intense rainfall—interact, leading to impacts that exceed the sum of their individual effects (Alipour et al. 2022). Approximately 18% of the world's population, equating to about one billion people, live in areas highly susceptible to TC-related mortality. Moreover, over a quarter of the global Gross Domestic Product is at significant risk of economic losses due to TCs (Dilley et al. 2005). When preparing for a severe weather event like TCs, emergency planners often evaluate a variety of "what if" scenarios to anticipate potential outcomes (Gombos and Hoffman 2013). In this study, we demonstrate one such "what-if" scenario—the "worst-case" scenario, which represents the event-wise maximum hazardous condition derived from TC forecast ensembles.

In recent years, numerical weather prediction centers, including the Japan Meteorological Agency (JMA), the National Centers for Environmental Prediction (NCEP) in the United States (US), and the European Centre for Medium-Range Weather Forecasts (ECMWF), have been generating TC track ensemble forecasts and incorporating them into operational settings (Swinbank et al. 2016). These forecast products are utilized by a wide range of user groups, extending beyond weather forecasting experts, and their economic advantages over deterministic forecasts (i.e., single best-guess forecasts) have been well-documented (e.g., Letson et al. 2007; Molina and Rudik 2024). In principle, a comprehensive approach to addressing the uncertainty in hazard intensity from an ensemble TC forecast would involve examining the potential hazard scenarios for each ensemble member. However, in case of TC, this approach is not practical or feasible, considering that forecasts consist of spatial patterns (Hoffman and Gombos 2012). Therefore, users are often restricted to relying on the ensemble mean or median hazard intensity (Titley et al. 2019). However, relying solely on the ensemble mean/median risks overlooking critical information about worst-case scenarios. This is particularly problematic, as many decision-making processes prioritize low-probability but high-impact worst-case events in the forecast (Scher et al. 2021). For instance, emergency service providers or local government may need to prepare large-scale evacuations in advance for worst-case TC scenarios. Moreover, in advance of a TC disaster, NGOs (e.g., the Red Cross) and businesses (e.g., insurance companies and hardware stores) may need to know worst-case spatial scenarios for efficiently allocating resources at a national level, encompassing provisions such as rescues, water, and food supplies. In such cases, an approach

that avoids the complexity of using every ensemble member but nevertheless captures potential worst-case scenarios can be highly valuable (Scher et al. 2021). Building on this idea, we explore a method to identify a subset of ensemble TC forecasts that represents a meaningful worst-case deviation from the ensemble mean, offering additional insights beyond those provided by the ensemble mean alone.

To explore how to derive a worst-case scenario from ensemble forecasts, we first define 'worst' as the condition that maximizes the estimated hazard intensity (e.g., storm surge, river flooding, gust wind) relative to the ensemble mean—in other words, values that are 'extreme' compared to other ensemble members. Depending on the forecast, these values may or may not represent extremes relative to the historical distribution of the hazard driver (e.g., storm surge) over a given period. This straightforward definition is sufficient for illustrating worst-case scenarios and holds practical relevance, as it aligns with approaches currently adopted by several operational forecasting agencies. For instance, JMA uses the maximum storm surge height at each location across six typical TC track forecasts (Hasegawa et al. 2017). In contrast, National Hurricane Center (NHC) in the US employs the surge height with a 10% probability of exceedance (NHC 2023; Sharma et al. 2022), while Bureau of Meteorology in Australia applies the 98^{th} percentile from an ensemble surge forecasts (Greenslade et al. 2017). These worst-case scenarios, being composite products, may be a reasonable approach for planning at a single locality. However, they are less suitable for generating a worst-case scenario across an entire region. This is because the varying meteorological conditions among different ensemble members (e.g., track, intensity, size, and translation speed) lead to an unrealistically large geographic area of extreme hazardous (e.g., storm surge) condition. In other words, the variability within the ensemble across different forecast locations is unlikely to exhibit strong positive correlations, except in the case of very small domains (Hoffman and Gombos 2012; Scher et al. 2021; Islam et al. 2023a). To overcome this shortcoming, several studies have proposed different methods that deal with the problem of interpreting ensemble forecasts and quantifying worst case scenarios. For example, Hoffman and Gombos (2012) introduced the concept of exigent analysis to derive TC induced worst wind damage scenarios constrained by the ensemble's statistical properties, ensuring that the results are dynamically consistent with the ensemble covariance structure. Scher et al. (2021) employed directional component analysis (DCA) as a novel statistical approach to identify extreme spatial patterns in ensemble forecasts. Unlike methods based on the worst single ensemble member or an average of extreme members, DCA identifies patterns that maximize likelihood while maintaining

physical plausibility. Although previous studies have been valuable for analyzing worst-case scenarios based on a single hazard, they are not equipped to address the complexities of multi-hazard worst-case scenarios (MHWCS) during TCs. In this context, adopting a multi-hazard framework is crucial, as it can enable disaster risk practitioners to comprehensively assess risks arising from interconnected hazards.

While the concept of a MHWCS is relatively new, related research has been conducted on compound extreme events (e.g., Sadegh et al. 2018; Gori et al. 2020). Compound extreme events involve multiple concurrent or consecutive hazard drivers (e.g., ocean and riverine flooding) that, while not necessarily extreme individually, can collectively result in substantial disaster impacts (Leonard et al. 2014; Wahl et al. 2015). Although MHWCS and compound extremes share similarities in addressing interactions between different hazard components, they differ fundamentally in several key aspects. First, studies on compound extremes typically rely on statistical techniques to analyze dependence structures (e.g., joint probability distributions, copula models) between hazard drivers, using historical datasets (e.g., Wahl et al. 2015; Sadegh et al. 2018). In contrast, MHWCS employs scenario-based methods to combine ensemble forecasts, identifying scenarios that represent potential worst-case risks across multiple hazards (e.g., storm surge, river flooding, gust wind speed). Second, compound extremes generally focus on concurrent or sequential events over short timescales (e.g., hours) and localized areas (e.g., Gori et al. 2020; Valle-Levinson et al. 2020), whereas MHWCS spans broader temporal and spatial scales, integrating hazards that may not occur simultaneously but collectively contribute to regional risk. Lastly, most compound extreme frameworks are limited to assessing risks from a pair of hazard drivers (e.g., storm surge and river discharge, or rainfall and wind; e.g., Messmer and Simmonds 2021; Du et al. 2024), while the MHWCS framework is more flexible and independent of specific hazard driver combinations. Consequently, understanding how to objectively integrate various TC-induced hazard drivers into a coherent and comprehensive forecast framework for defining MHWCS remains a significant challenge, requiring further exploration beyond the existing methods for compound extremes.

In this study, we aim to enhance the utility of ensemble TC forecasts by building on our previously proposed single-hazard based objective quantification of worst-case scenarios (Islam et al. 2023a) and introducing a framework for Multi-Hazard Worst-Case Scenario (MHWCS) assessment, for the first time. We present a novel approach based on Pareto-optimality to evaluate storm surge, river flooding, and gust wind-induced MHWCS using

ensemble TC forecasts. Our methodology advances existing assessment techniques by employing a multi-objective function alongside affinity propagation, an advanced clustering algorithm, to identify meaningful MHWCS and quantify multi-hazards for Tokyo, Japan. Our approach involves a comprehensive analysis of Pareto-optimal solutions to explore how forecasted TC meteorological variables—such as rainfall, track, intensity, size, and translation speed—affect to produce MHWCS. To demonstrate the framework, we used an extremely large ensemble forecasts (1,000 members) of TC Hagibis, which made landfall in Japan in 2019. The proposed approach will enable forecasters to efficiently predict MHWCS from ensemble TC forecasts and serve as a valuable tool for emergency responders to prepare for multi-hazard scenarios effectively.

2. Data and methods

a. TC Hagibis and ensemble forecasts

TC Hagibis, one of the most destructive and deadliest cyclones to impact Japan in decades (Ma et al. 2021; Shimozono et al. 2020), was selected to demonstrate our MHWCS assessment. Hagibis formed over the western North Pacific Ocean on October 2, 2019, and made landfall in Japan, near Tokyo (Fig. 1) on October 12, 2019, at approximately 09:00 UTC. At landfall, TC's 10-minute maximum sustained wind speed reached 80 kt. Combined with strong winds and intense rainfall, Hagibis triggered significant storm surges, widespread flooding, and wind disaster in the region and resulted in 86 deaths, three missing persons, nearly 500 people injured, and approximately 400 billion dollars of damage (JMA 2021; Ma et al. 2021).

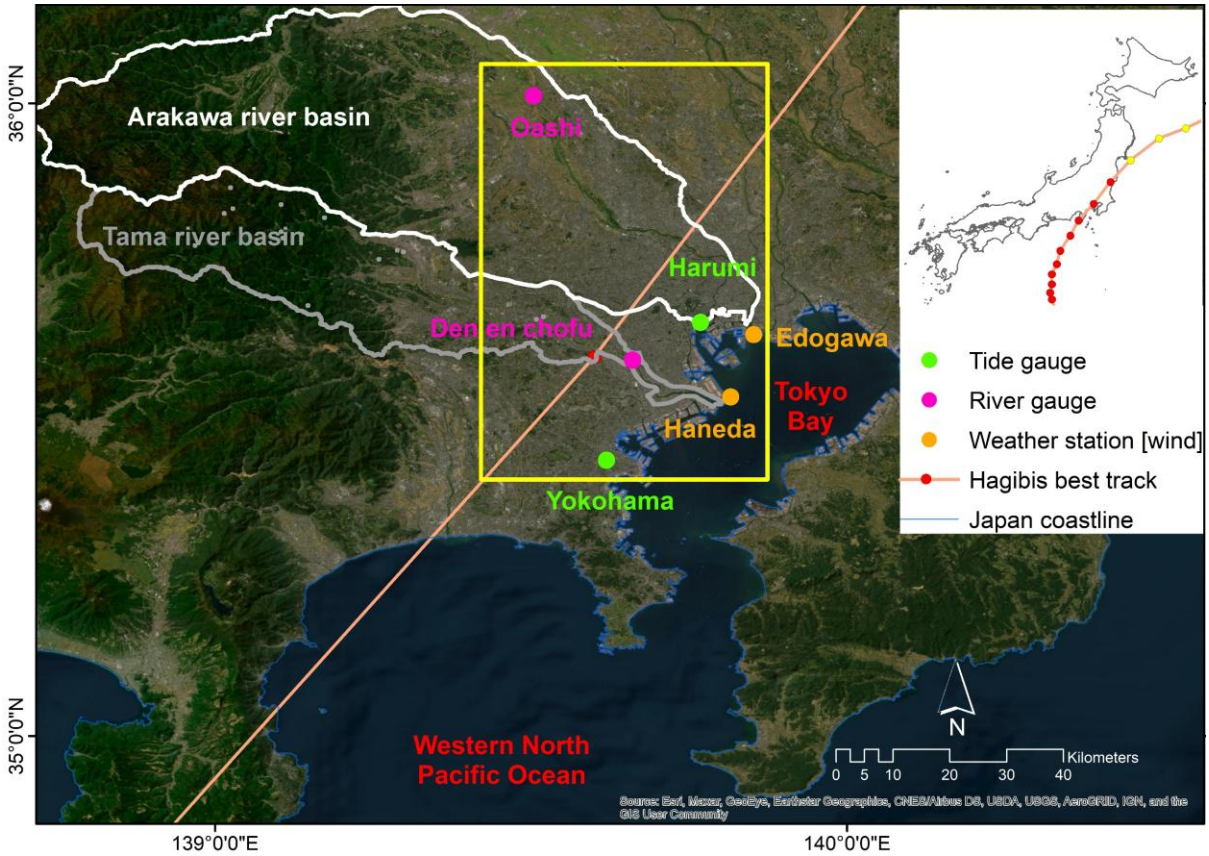

FIG. 1. Domain of the multi-hazard forecasts in Tokyo and the locations of the weather station (wind), tide, and river gauges used for gust wind, storm surge, and flood model validation and forecasts, respectively.

The atmospheric ensemble forecasts for TC Hagibis were generated using JMA's former operational limited-area nonhydrostatic model (NHM; Saito et al. 2006) . The model domain had a horizontal resolution of 5 km, with 817 × 661 grid points and 50 vertical levels. Boundary conditions were derived from JMA's operational global model forecasts, with boundary perturbations obtained by the method described in Duc et al. (2021).

Since we used NHM for all forecast members, uncertainty in the forecasts stemmed solely from initial and boundary conditions. Initial conditions were based on error covariances of the atmospheric state, estimated through a four-dimensional variational-ensemble assimilation technique (4DEnVAR; Liu et al. 2008) with a large ensemble size of 1,000 members. Localization is needed to reduce sampling noise in background error covariances, however, localization at the same time can distort the coherent vertical structure between atmospheric fields, critical for TC prediction. As the ensemble size was large, localization was relaxed by retaining vertical correlations as determined by ensemble members and removing horizontal correlations at distant locations (Duc et al. 2021). The horizontal localization length scale, i.e., the distance at which horizontal correlations are tapered to zero, was set to 700 km.

The assimilation system began at 00 UTC on October 7, 2019, and ran with a 3-hour assimilation cycle until 18:00 UTC on October 10, 2019. The resulting analysis ensemble was used as the initial condition for 39-hour NHM forecasts, matching the forecast horizon of JMA's operational Mesoscale Ensemble Prediction System (MEPS; Ono et al. 2021; JMA 2023a). Routine observations from JMA's database were assimilated across the forecast domain, ensuring consistency between the assimilation and forecast settings. Further methodological details, including the unique implementation of 4DEnVAR for generating analysis perturbations without relying on an ensemble Kalman filter, can be found in Islam et al. (2023).

b. Ensemble storm surge forecasts

In this study, we employed the storm surge hazard potential index (SSHPI; Eq. 1; (Islam et al. 2021, 2023a)), a statistical model designed to estimate peak storm surge height based on key meteorological and geographical variables. The SSHPI incorporates TC intensity as maximum sustained wind speed (V_{max}), size (radius of 50-kt wind, R_{50}) and translation speed (S), as well as factors such as coastal geometry (a), landfall location sensitivity (D_L), and regional bathymetry (L_{30}). Reference constants (V_{ref}, R_{ref}, and S_{ref}) represent typical historical values of 50-kt winds, 95 nautical miles (nm) for R_{50}, and 35 km/h for S during landfall in mainland Japan (Islam et al. 2021). Full details of the SSHPI formulation and parameter definitions can be found in our earlier studies (Islam et al. 2021, 2022, 2023b,a). The formulation of the SSHPI is the following:

$$\text{SSHPI} = \left(\frac{V_{max}}{V_{ref}}\right)^2 \left(\frac{R_{50}}{R_{ref}}\right) \left(\frac{S}{S_{ref}}\right)^a \left(\frac{L_{30}}{L_*}\right) (D_L) \qquad (1)$$

$$\frac{R_{50}}{R_{ref}} = \begin{cases} 1.5 & if\ \frac{R_{50}}{R_{ref}} \geq 1.5 \\ \frac{R_{50}}{R_{ref}} & if\ 0.5 < \frac{R_{50}}{R_{ref}} < 1.5 \\ 0.5 & if\ \frac{R_{50}}{R_{ref}} \leq 0.5 \end{cases} ; \left(\frac{S}{S_{ref}}\right)^a = \begin{cases} 1.5 & if\ \left(\frac{S}{S_{ref}}\right)^a \geq 1.5 \\ \left(\frac{S}{S_{ref}}\right)^a & if\ 0.5 < \left(\frac{S}{S_{ref}}\right)^a < 1.5 \\ 0.5 & if\ \left(\frac{S}{S_{ref}}\right)^a \leq 0.5 \end{cases} ; \frac{L_{30}}{L_*} = \begin{cases} \frac{L_{30}}{L_*}, & if\ \frac{L_{30}}{L_*} \geq 1 \\ 1, & if\ \frac{L_{30}}{L_*} \leq 1 \end{cases}$$

$$D_L = \begin{cases} 1 & if\ the\ surge\ estimated\ point\ falls\ right\ side\ of\ TC\ track\ and\ x \leq 20 \\ & OR \\ & if\ the\ surge\ estimated\ point\ falls\ left\ side\ of\ TC\ track\ and\ x \leq 10 \\ 1 - \dfrac{0.03(x-20)}{20} & if\ the\ surge\ estimated\ point\ falls\ right\ side\ of\ TC\ track\ and\ x > 20 \\ 1 - \dfrac{0.05(x-10)}{10} & if\ the\ surge\ estimated\ point\ falls\ left\ side\ of\ TC\ track\ and\ x > 10 \end{cases}$$

In this study, ensemble forecasts of TC Hagibis (1,000 members) were used as meteorological forcing for the SSHPI, focusing on the landfall period, when storm surge amplification typically occurs (Islam et al. 2021, 2022, 2023b). However, the peak surge may not always coincide with landfall characteristics, as surge heights can be higher when the TC track is closer to enclosed areas, such as inner Tokyo Bay. This may introduce some uncertainties in the surge estimations. Furthermore, SSHPI does not include the inverse barometer effect, wave setup, and astronomical tides to maintain simplicity. While this approach may lead to some errors in estimating surge heights, it is found suitable for ensemble-based analyses as shown in Islam et al. (2023a).

We produced 1,000 perturbed peak surge forecasts with a 39-hour lead time. Figure 1 illustrates the location of tide gauges used for both validating the surge model and forecasting surge hazards. It should be noted that the tide gauges selected for this study are the only stations with recorded historical storm surge data in Tokyo, maintained by JMA (2022). The bathymetry for the target region was sourced from the Japan Oceanographic Data Center (2020). Empirical relationships between SSHPI and observed surge data at the selected tidal stations, developed in prior studies (Islam et al. 2021, 2022, 2023b), were used for forecasting storm surge hazards in this study.

c. Ensemble flood forecasts

We employed the Runoff Index Model (RIM), the operational flood forecasting model used by the JMA for medium- and small-sized rivers (21,394 rivers) in Japan (Tanaka et al. 2008; Ota 2017; Ota and Makihara 2018; Ota et al. 2023). RIM serves as the basis for issuing flood advisories and warnings. The model consists of two primary components: the runoff component, which simulates rainfall flowing into rivers, and the river routing component, which models rainfall flowing downstream. The runoff component employs a tank model structure, comprising three tanks (surface, midstream, and groundwater) for non-urban areas and five tanks for urban areas. These tank models are positioned at 1 km intervals across Japan. The river routing process is simulated using Manning's roughness formula, enabling the calculation of river discharge.

RIM generates an output termed the "Index," which is used to issue flood advisories and warnings based on predefined "Criteria Levels" (levels 1–3). The "Index" is defined as the square root of river discharge at each river channel grid point, which is computed using the runoff and river routing models. Rather than explicitly accounting for factors such as dams,

levees, river confluences, tides, and other influences on river discharge, RIM integrates these effects indirectly through the "Criteria Levels". These levels are calibrated using historical flood events from heavy rainfall cases since 1991 and are further adjusted to reflect the impact of infrastructure and additional flooding mechanisms, such as backwater effects and tides. For example, if a new dam is constructed upstream, the Criteria Level values will be set higher. Conversely, if a levee is breached, the Criteria Levels are adjusted lower. The JMA and local governments review and adjust these Criteria Levels for all rivers annually.

Geographic data including river channels, geology, slope, and land use, are made from the National Land Information System. The conceptual foundation of RIM aligns with the principles of impact-based forecasting and warning systems. Full details including the operational performance of the RIM are available in earlier studies (Ishihara and Kobatake 1979; Tanaka et al. 2008; Ota 2017; Ota and Makihara 2018; Ota et al. 2023).

In this study, the spin-up run of the RIM model was conducted from 00:00 UTC on September 1, 2019, to 18:00 UTC on October 10, 2019, using rainfall observations from the JMA Radar-AMeDAS system (hereafter RA; Nagata 2011). The ensemble flood forecast simulation spanned from 18:00 UTC on October 10, 2019, to 23:00 UTC on October 12, 2019. Each 54-hour forecast for all rivers in Japan required one node and approximately 10 minutes of computational time per ensemble member. The forecasts utilized precipitation data derived from the ensemble TC forecasts, which were interpolated to the RIM domain with a spatial resolution of 1 km. While the RIM computed the flood index for approximately 21,000 rivers across Japan, two specific grid points within the study area (Fig. 1) were selected for validation and flood hazard forecasting. These points correspond to two river gauges: Oashi-bashi (hereafter, Oashi), located upstream in the Arakawa River basin (2,940 km^2), and Den-en-chofu, situated downstream in the Tama River basin (1,240 km^2; Fig. 1). These gauges represent two primary rivers flowing through Tokyo. The selection of these locations was based on record-breaking river water levels observed since monitoring began by the Ministry of Land, Infrastructure, Transport, and Tourism, Japan (MLIT 2024), as well as documented flood disasters in the respective areas (Das et al. 2020). While the forecasts provided a complete hydrograph of the flood index, this study focuses on the forecasted peak flood index from each ensemble member for the assessment of MHWCS. Although river engineers and hydrologists are often concerned with the complete flood hydrograph, decision-makers responsible for

issuing flood warnings and coordinating relief measures primarily focus on the predicted peak flood water level.

d. Ensemble gust wind forecasts

Our ensemble TC forecasts did not directly estimate gust wind factors. To address this, we derived gust wind speeds using the JMA (n.d.) wind force scale, which provides an empirical relationship between the average wind speed over a 10-minute period and the maximum gust wind speed that could occur on land, as summarized in Table 1. Figure 1 shows the locations of the JMA-operated weather stations (Haneda and Edogawa), which were used for both validation and forecasting of gust wind. These two stations were specifically chosen because of their proximity to Tokyo Bay and their reduced susceptibility to terrain-features compared to other weather stations in Tokyo. Although the 1,000-member ensemble forecasts produced time series data for gust wind, this study focuses on the forecasted maximum gust wind speed from each ensemble member as a representative measure for the worst wind hazard scenario.

TABLE. 1. JMA (n.d.) wind force scale

Average wind speed (kt) on land	Maximum gust wind speed (kt) on land	Wind strength
19-29	39	Moderate gale
30-39	58	Gale
40-58	78	Storm
59-68	97	Violent storm
69-78	117	Violent storm

e. Pareto optimality and assessing MHWCS

In an ensemble TC forecast, the worst-case scenario is not likely to occur simultaneously at all forecast locations across a region. This is because the variability in the forecast (e.g., differences in wind speed and rainfall) tends to distribute extremes unevenly across different areas, except in the case of very small domains. The best we can do is to quantify the trade-off between different hazard intensities across different locations. Here, we performed multi-objective optimization to identify ensemble forecast members (among 1,000 ensemble forecasts) that effectively represent the potential worst-case scenario induced by TC Hagibis

in Tokyo (Fig. 1) by calculating the Pareto frontier. The Pareto frontier represents the trade-offs between multiple objectives and consists of all Pareto-optimal solutions.

In this study, we analyzed a subset of 1000 forecasted hazard scenarios (e.g., river flooding, storm surge, gust wind) for each forecast location in Tokyo (Fig. 1), referred to as solution *z*. Each scenario was evaluated based on *m* objectives (*m*-dimensional), represented as $y^1(z)$, $y^2(z), \ldots\ldots, y^m(z)$. As an example, in the case of the worst river flooding scenario, the objectives were to maximize the forecasted peak flood index at two river gauges: Den-en-chofu ($y^1(z)$) and Oashi ($y^2(z)$). This objective function aimed to identify potential worst-case flooding scenarios relative to ensemble mean from the 1,000 ensemble flood forecasts. In this multi-objective optimization, the criterion space (the set of all objective values) was two-dimensional. To objectively compare two scenarios, *z* and *z′*, a ranking was established based on dominance. Scenario *z* dominates *z′* if and only if $y^i(z) \geq y^i(z')$ for $i \in \{1, 2\}$ and $y^i(z) > y^i(z')$ for at least one objective. Using this framework, we identified Pareto-optimal solutions from the 1,000 scenarios. A Pareto-optimal solution represents a scenario where no other solution can improve one objective without compromising another. These solutions lie on the boundary of the criterion space and may result in multiple non-dominated (optimal) solutions, reflecting trade-offs between objectives. Each Pareto-optimal solution represents a distinct but equally valid outcome among competing criteria. In such cases, there is no single "best" worst case scenario, and a set of solutions should be analyzed. Similarly, an objective function was defined to minimize the forecasted peak flood index at the two river gauges, enabling the identification of ensemble members that characterize potential minimum flood scenarios. We repeated the same analyses for other hazard components: storm surge and gust wind. The advantages of this method from a single hazard perspective are discussed in detail in Islam et al. (2023a).

Building upon the single-hazard framework, we extended this methodology to a multi-hazard perspective for assessing MHWCS. This extension integrated forecasts of flood ($y^1(z)$ and $y^2(z)$), storm surge (Harumi: $y^3(z)$ and Yokohama: $y^4(z)$), and gust wind (Haneda: $y^5(z)$ and Edogawa: $y^6(z)$) hazards, creating a six-dimensional criterion space where the objective function is to maximize $\{y^1(z), y^2(z), y^3(z), y^4(z), y^5(z), y^6(z)\}$. A scenario *z* is Pareto-optimal if no other scenario *z′* exists such that:

$$y^i(z') \geq y^i(z),\ i \in \{1, 2, 3, 4, 5, 6\}$$

with at least one inequality being strict. Here, a strict inequality (>) means that z' must outperform z in at least one objective to dominate it. This ensures that z is not entirely surpassed by any other scenarios in the forecast and thus, z lies on the Pareto frontier. As discussed above, the Pareto frontier may include several non-dominated solutions, representing the appropriate trade-offs among the hazard components.

Unlike single-hazard-based worst case scenarios, not all identified Pareto-optimal solutions for MHWCS represent the worst-case across all hazard components, as 'worst' is defined here as the condition that maximizes the estimated hazard intensity relative to the ensemble mean. For instance, maximizing $y^1(z)$ and $y^2(z)$, might compromise worst $y^5(z)$ and $y^6(z)$ or worst $y^3(z)$ and $y^4(z)$, and vice versa. To refine the analysis, we further sampled Pareto-optimal solutions using an advanced clustering algorithm called affinity propagation and assessed the hazardousness of each cluster across all hazard components. Affinity propagation uses measures of similarity between pairs of data points as input and iteratively exchanges real-valued messages between these points until a high-quality set of clusters is formed. This clustering algorithm does not require the number of clusters to be specified beforehand, and it has been found to be advantageous over related techniques such as *k*-means clustering, expectation-maximization, hierarchical agglomerative clustering, and spectral clustering for various applications (Frey and Dueck 2007). While each MHWCS (Pareto-optimal solutions) represents a unique balance among the competing hazard objectives, affinity propagation-based evaluation utilized to identify a special cluster (a set of Pareto-optimal solutions) that maximizes the deviation from the ensemble mean across the six forecast locations selected in this study.

3. Results

a. model evaluation

1) TC AND STORM SURGE ENSEMBLE FORECASTS AND VALIDATION

In the previous study (Islam et al. 2023a), we have compared and validated our 4DEnVAR based TC Hagibis forecasts (39-h lead time) with JMA's operational 21-member ensemble forecast (Meso-scale Ensemble Prediction System; MEPS). It demonstrated superior track prediction accuracy, with the ensemble mean closely aligning with the best track and exhibiting smaller distance errors compared to MEPS. Our forecast systematically underestimated (~ 5-kt) V_{max}, particularly at earlier forecast times (forecast hours 3–30). However, during the

landfall period (forecast hours 33–39), the forecasts converged closer (~3-kt) to the best track estimates.

Similar to the evaluation of ensemble TC forecasts, we compared and validated the 1,000 ensemble-based storm surge predictions with the JMA best track estimate, as detailed in Islam et al. (2023a). The analysis revealed that both the ensemble mean forecasts in 39-h lead time and the best track estimates consistently underestimated (~5 cm) the observed peak surge levels. However, the observed peak surge values were encompassed within the full ensemble spread at both tide gauge locations (Harumi and Yokohama), indicating that the ensemble spread was sufficiently large to capture the uncertainty in the predictions. The mean absolute error across the two stations is 6.7 cm. Further details on the track, intensity, and storm surge forecasts are provided in Islam et al. (2023a).

2) RIVER FLOOD FORECASTS VALIDATION

Figure 2 presents the evaluation of the RIM using 1,000 ensemble flood forecasts, with RA serving as the ideal input data for flood forecasting at two water level observation points: Den-en-Chofu and Oashi. The average hourly rainfall amounts (purple bars) for the Tama River (Fig. 2a) and the Arakawa River (Fig. 2b) exceeded 10 mm between 07:00 and 22:00 JST on October 12, indicating prolonged periods of very heavy rainfall in both basins. The peaks of the RA index (red line) and the water level observations (green line) occurred almost simultaneously, suggesting that the RIM, when using RA as input, could accurately reproduce the observed flood conditions.

Figures 2a and 2b reveals that the ensemble forecast underpredicted the RA forecast at both observation points until 19:00 JST on October 12. After that, the 1,000-member ensemble forecast began to be similar to the RA forecast. Notably, at Oashi (Fig. 2b), the RA forecast exhibited a pronounced increase in the index starting at 10:00, while the ensemble forecast showed a similar increase with a delay, between 13:00 and 15:00. This discrepancy is likely due to deviations in the TC track and translation speed as predicted by the meteorological model. The upper basin of Oashi, with an area of 1,019 km², poses challenges for accurate rainfall forecasting, even with the large 1,000-member ensemble. It is hypothesized that the 5-km resolution of the model may not be sufficient for capturing localized heavy rainfall events. Previous studies have emphasized that higher resolution is critical for effective heavy rain forecasting in Japan (e.g., Oizumi et al. 2018, 2020). In contrast, the Den-en-Chofu observation point, located downstream on the Tama River, exhibited less deviation between the RA and the

1,000-member ensemble forecasts, as shown in Fig. 2a. The exceedance probabilities at both observation points indicates that over 75% of the ensemble members at both locations predict a risk of surpassing the previous maximum flood index. Nevertheless, RIM's flood risk ensemble forecast has a satisfactory accuracy to be used for scenario-based analysis.

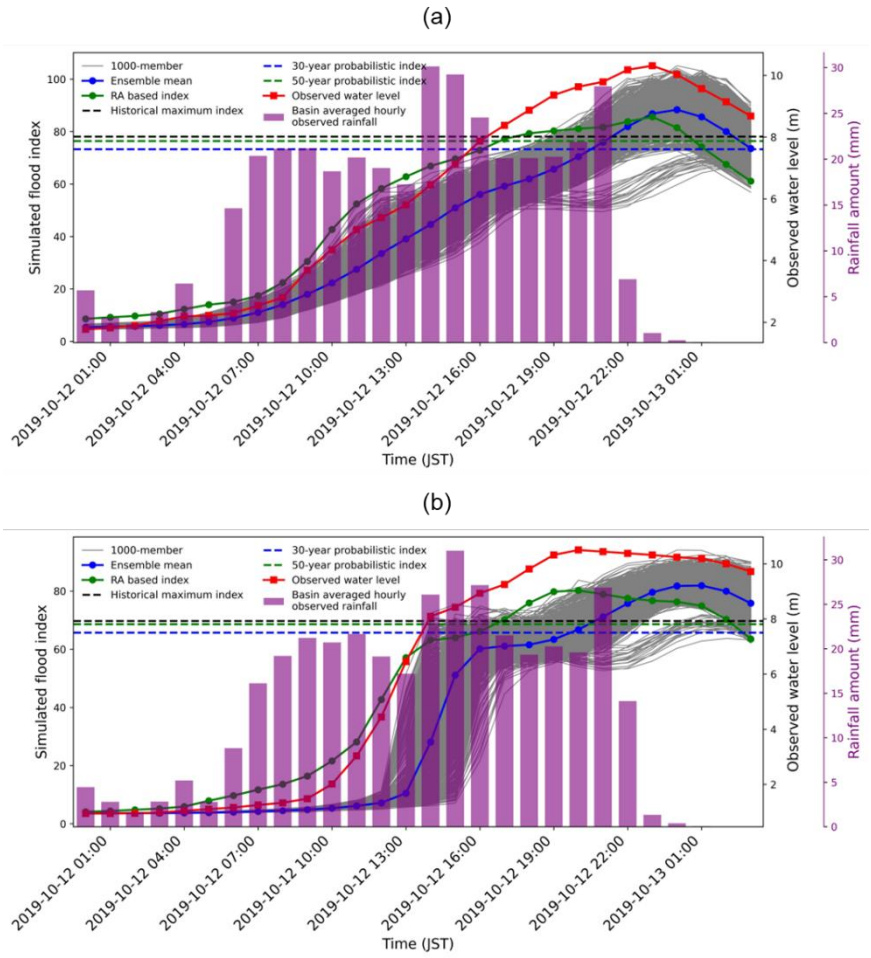

FIG. 2. A comparison of the RIM based 1,000 ensemble flood index forecasts (ensemble member: gray lines; ensemble mean: blue line) in 39-h lead time and the flood index using Radar AMeDAS system (green line) for TC Hagibis at two river gauges: (a) Den-en-chofu; (b) Oashi. The observed river water level respective to each river gauge is indicated by a red line. The basin averaged hourly observed rainfall (purple bars) corresponds to Tama River (a) and Arakawa River (b). Historical maximum index, 30-year probabilistic index, and 50-year probabilistic index respective to each river gauge are indicated by a dotted black, blue, and green line, respectively.

3) GUST WIND SPEED FORECASTS VALIDATION

Figure 3 compares the observed maximum hourly gust wind speeds with a 1,000-member ensemble forecast in 39-h lead time at two weather stations: Edogawa (Fig. 3a) and Haneda (Fig. 3b). For each hour, the observed gust wind speed was determined by sampling six

measurements recorded at 10-minute intervals by JMA (2024) and selecting the maximum value (red dots). The ensemble forecast data are represented by the ensemble mean (blue dots) and a vertical range (black bars) spanning the minimum to maximum gust wind speeds predicted by the 1,000 ensemble members. At both weather stations, the uncertainty range increases with forecast lead time. During earlier forecast hours (01:00–05:00 JST on 12 October), the forecasts overestimated the observed maximum gust wind speeds. Around the time of TC landfall (approximately 18:00 JST on 12 October), the observed gust wind speeds generally fell within the ensemble's range, indicating that the forecast envelope effectively captured the actual conditions as the TC approached land. The mean absolute error across two stations during landfall is 3.4-kt. In other instances, the observed gust exceeded the upper limits of the ensemble range limits, highlighting circumstances where the empirical estimate underestimated the maximum gust wind speed.

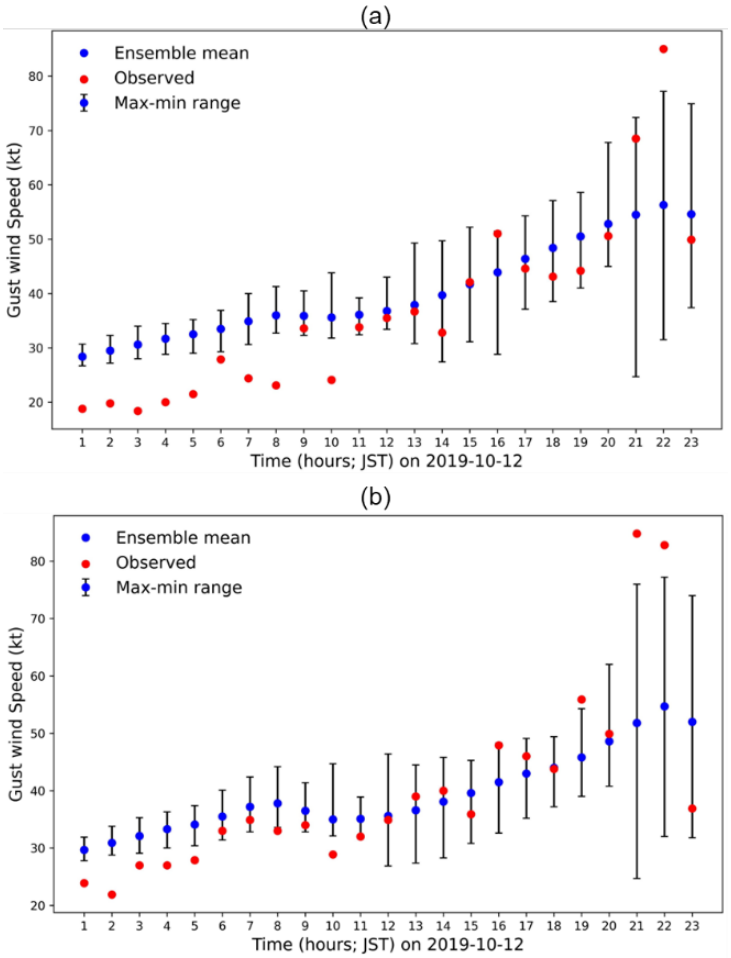

FIG. 3. A comparison of the 1,000 ensemble gust wind forecasts and observed hourly peak gust wind speed (red dot) for TC Hagibis at two weather stations: (a) Edogawa; (b) Haneda. The hourly ensemble mean is

indicated by a blue dot and max-min range is determined from 1,000 ensemble gust wind forecasts for each forecast hour respective to each weather station.

b. Multi-scenario analysis

1) PARETO-OPTIMAL MULTI-SCENARIOS

The Pareto-optimal frontier, as shown in Fig. 4, illustrates a set of solutions that highlight the forecasted potential worst and optimal scenarios from a single-hazard perspective for TC Hagibis in Tokyo. For example, the two-dimensional Pareto frontier (Fig. 4a) allows for a clear evaluation of the trade-offs between forecasted peak flood indices at two different river basins. The results identify the appropriate ensemble members from the 1,000 TC forecasts to represent the potential worst-case flood scenario (Den-en-chofu: ~ 97.5; Oashi: ~ 90.1) and the optimal scenario (Den-en-chofu: 66.1; Oashi: ~63.7). The location of the river gauges (Den-en-chofu and Oashi) are geographically distant (Fig. 1) and exhibit differing hydrological characteristics, such as river gradients. As a result, the relationship between the predicted peak flood indices in the two locations are not fully linear, leading to diverse trade-offs among the worst-case flood outcomes within the Pareto frontier (Fig. 4a). A similar pattern is also observed for gust wind forecasts across the two weather stations (Fig. 4c). In contrast, a strong linear relationship is evident in the worst storm surge forecasts for inner Tokyo Bay (Fig. 4b), as the two locations share similar coastal geometries, including bathymetry, and are situated close to each other (Fig. 1). It is important to note that no commonality exists in the Pareto-optimal solutions presented in Fig. 4 across all hazard components. This indicates that the ensemble member producing the worst flood hazard does not necessarily result in the worst storm surge or gust wind hazard for Tokyo, and vice-versa.

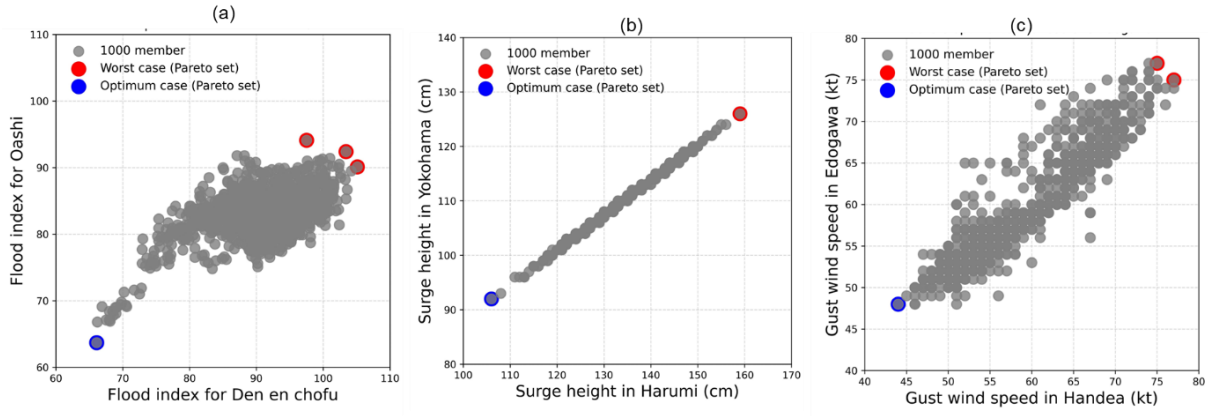

FIG. 4. Forecasted Pareto-optimal multi-scenarios in 39-h lead time due to TC Hagibis, apply for (a) flood hazard in Den-en-chofu and Oashi (objective function (red dot): max flood index in Den-en-chofu and Oashi;

objective function (blue dots): min flood index in Den-en-chofu and Oashi); (b) storm surge hazard in Harumi and Yokohama (objective function (red dot): max surge height in Harumi and Yokohama; objective function (blue dots): min surge height in Harumi and Yokohama); (c) wind hazard in Haneda and Edogawa (objective function (red dot): max gust wind in Haneda and Edogawa; objective function (blue dots): min gust wind in Haneda and Edogawa).

Figure 5 shows forecasted multi-hazard scenarios for TC Hagibis in Tokyo. Unlike the single hazard framework (Fig. 4), it is unrealistic to anticipate a "nice" forecast scenario that maximizes hazard intensity across all components at all locations due to the existence of a large number of Pareto optimal solutions (= 153; red lines in Fig. 5). This diversity arises from the trade-offs among hazard components, each driven by distinct physical mechanisms and influenced by different TC meteorological conditions. For instance, some Pareto optimal solutions in Fig. 5 predict worst storm surge levels exceeding 150 cm at Harumi and 120 cm at Yokohama, while under the same scenarios, Den-en-chofu (Oashi) and Haneda (Edogawa) experience significantly lower hazard magnitudes—less than 86 (77) for the flood index and 55 kt (60 kt) for maximum gust wind, respectively. These flood index (~86) and gust wind speed (~55 kt) values are notably lower than those predicted by other Pareto-optimal solutions for worst-case flood and wind hazards in Fig. 5. Likewise, 41% of the Pareto optimal solutions (= 62) predict worst-case scenarios at any two forecast locations where the respective hazard magnitudes are lower than the 1,000-ensemble mean.

This complexity becomes even more apparent when analyzing the correlations across the 1,000 ensemble multi-hazard forecasts. As shown in Fig. 6, none of the hazard components exhibit strong associations with each other, with Pearson correlation coefficients below 0.25. This highlights that the worst-case scenario for one hazard component often does not align with the worst-case scenario for other components. Consequently, the lack of strong correlations and the independent behavior of different hazard components lead to a large number of Pareto-optimal solutions in our forecast framework. This emphasizes the importance of considering multiple scenarios when issuing warnings and assessing the risks posed by extreme weather events like TCs.

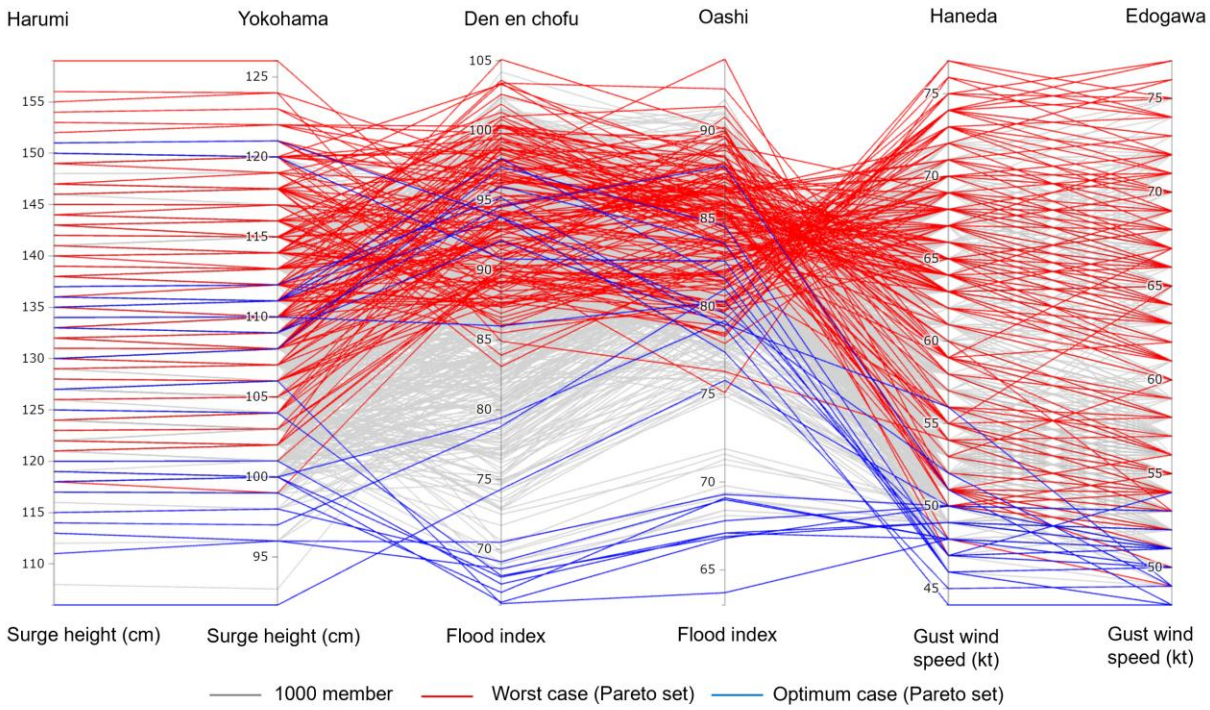

FIG. 5. Forecasted Pareto-optimal MHWCS in 39-h lead time due to TC Hagibis in Tokyo using the parallel coordinate plot [objective function (red lines): max surge height in Harumi and Yokohama + max flood index in Den-en-chofu and Oashi + max gust wind speed in Haneda and Edogawa; objective function (blue lines): min surge height in Harumi and Yokohama + min flood index in Den-en-chofu and Oashi + min gust wind speed in Haneda and Edogawa]. In this plot, each parallel line represents a hazard component, with coordinates marking hazard magnitudes, and the red (blues) lines connecting these values represent individual Pareto-optimal solutions for MHWCS (multi-hazard optimum cases). The remaining grey lines correspond to TCs that are not Pareto optimal.

While each MHWCS shown in Fig. 5 (red lines) represents a unique trade-off among the competing hazard objectives, we further refined the assessment by applying the affinity propagation clustering algorithm. This allowed us to identify a subset of Pareto-optimal solutions (a special cluster) that maximizes worst-case deviations from the ensemble mean. Figure 7 illustrates the resulting 12 clusters of MHWCS, where the number of clusters was not pre-specified. Instead, the clustering process relied on the message-passing method inherent to affinity propagation, which determined the appropriate number of clusters (12 in this case) automatically.

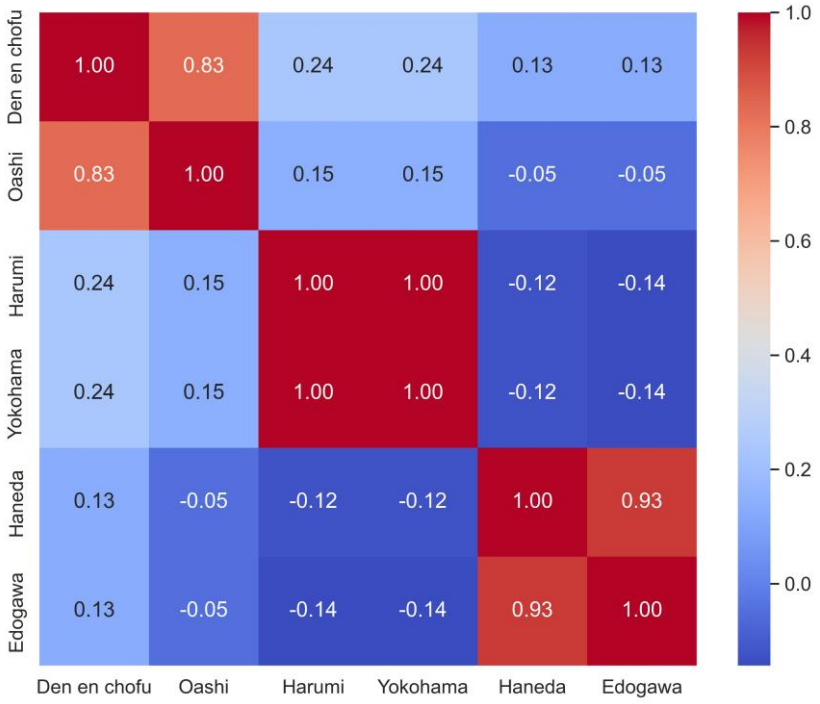

FIG. 6. Multivariate correlation (Pearson) matrix for three hazard components in 1,000-ensemble forecasts: storm surge, flood, and gust wind across six forecast locations.

To assess how effectively this clustering approach identifies a subset of Pareto-optimal solutions, we evaluated multi-hazard intensities of each cluster with respect to their deviation from the 1,000-ensemble mean hazard intensity. We define the special cluster of MHWCS as the highest percentage of ensemble forecasts in each cluster that deviates from the ensemble mean hazard intensity. Overall, the ensemble mean (black line marker in Fig. 7) of the 153 MHWCS exceeds the 1000-ensemble mean (blue line marker in Fig. 7). However, with the exception of cluster (i) in Fig. 7 (red lines), all other clusters include some ensemble members that predict worst-case scenarios at two or more forecast locations where the respective hazard magnitudes fall below the 1,000-ensemble mean. For instance, clusters (c), (g), and (k) forecast the most severe cases for flood hazards (e.g., similar to Fig. 4a), storm surge (e.g., similar to Fig. 4b), and wind hazards (e.g., similar to Fig. 4c) in Tokyo, respectively. However, several ensemble members within these clusters predict lower intensities of other hazard components compared to the 1,000-ensemble mean. On the other hand, our clustering analysis effectively identifies cluster (i), consisting of 18 Pareto optimal solutions, as the special cluster of MHWCS. Given the definition of special cluster, each Pareto-optimal solution in cluster (i) in Fig. 7 (red lines) exceeds the 1000-ensemble mean. Therefore, cluster (i) maximizes multi-hazard intensity across all the six forecast locations compared to the solutions in the other clusters (Fig. 7a–h, j–l). In addition to multi-hazard intensities, Fig. 7(i) also provides

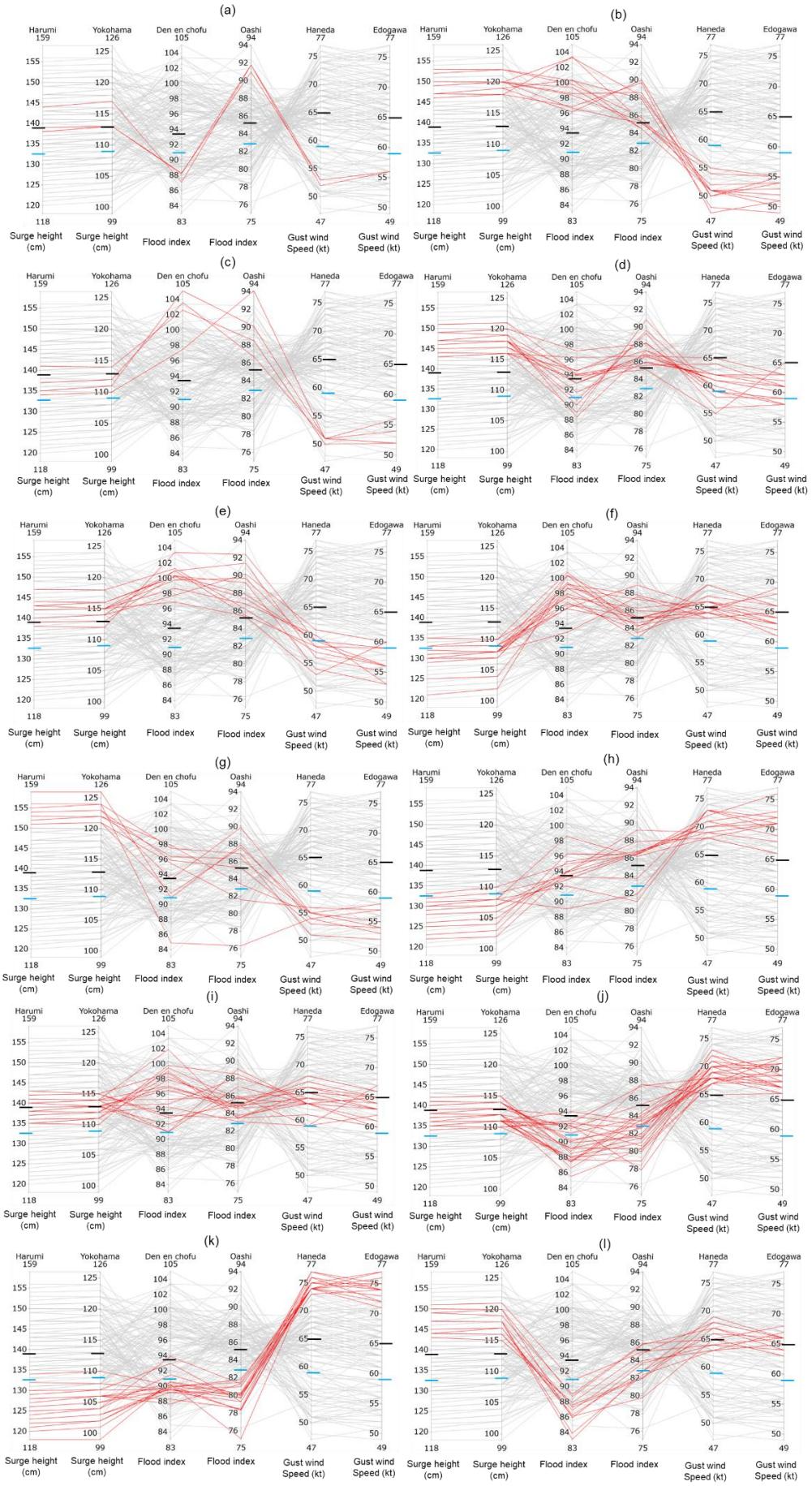
(a)
(b)
(c)
(d)
(e)
(f)
(g)
(h)
(i)
(j)
(k)
(l)
Harumi
Yokohama
Den en chofu
Oashi
Haneda
Edogawa
Surge height (cm)
Flood index
Gust wind Speed (kt)

FIG. 7. (a-l) Twelve clusters identified by affinity propagation from 153 Pareto optimal solutions (MHWCS in Fig. 5) are color coded in red. Each parallel line represents a hazard component, with coordinates marking hazard magnitudes, and the grey lines connecting these values correspond to individual Pareto-optimal solutions (among 153 MHWCS) that are not included in the cluster sub-set. The black and blue line markers on each parallel line represent ensemble mean hazard intensity derived from the 153 MHWCS and the 1,000-enssemble hazard forecasts, respectively.

uncertainty ranges for the special cluster of MHWCS, offering a more comprehensive understanding of potential scenarios. It is noteworthy that this special set of Pareto-optimal solutions does not necessarily represent the most extreme events from a single-hazard perspective. For example, Fig. 7(i; red lines) predicts a maximum flood index of 101.9 (89.1) at Den-en-chofu (Oashi), a surge level of 143 cm (115 cm) at Harumi (Yokohama), and gust wind speeds of 68 kt (67 kt) at Haneda (Edogawa). These values are approximately 3% (~5%), 10% (~9%), and 12% (~13%) less severe, respectively, than the worst-case scenarios depicted in Fig. 4a–c (red dots). Nevertheless, the interdependence among the three hazard drivers shown in Fig. 7(i) is forecasted to trigger significant multi-hazard impacts, highlighting the critical importance of identifying special set of Pareto-optimal solutions.

2) TC METEOROGICAL VARIABLES AND TRACK ANALYSIS OF MHWCS

To understand which combinations of TC meteorological variables contribute to the worst case scenarios shown in Fig. 7, we analyzed the forecasted key meteorological variables (Fig. 8) and tracks (Fig. 9) associated with Pareto optimal solutions. Figure 8 (i-v) illustrates the cluster-wise distributions of (i) translation speed (S), (ii) radius of 50-kt wind (R_{50}), (iii) mean sea level pressure (MSLP), (iv) maximum wind speed (V_{max}), and (v) basin averaged accumulated rainfall, at the time of landfall or when the track passed closest to the study area. Among these variables, translation speed emerged as the strongest single predictor of single-hazard worst-case scenarios (Fig. 8 (vi)). For example, cluster (c) in Fig. 7, which is associated with slower S (Fig. 8 (i)), forecasts the most severe flood cases, in contrast to cluster (k), which exhibits faster-moving ensembles (Fig. 8 (i)). The distinct differences in flooding intensity between these two clusters can be largely attributed to variations in rainfall accumulation. As shown in Fig. 8 (v), the river basins in cluster (c) are forecasted to receive 26% more rainfall compared to those in cluster (k). This disparity aligns with the differences in translation speed—Fig. 8 (i) reveals that the forecasted mean S in cluster (c) is 18% slower than in cluster (k). Given that other meteorological variables (Fig. 8 (ii-iv)) remain relatively similar, the slower-moving ensembles in cluster (c), passing closer to the study area (Fig. 9), likely resulted

in higher rainfall amounts and consequently, an increased risk of flooding. This tendency becomes apparent when *S* and flooding intensity exhibits association with each other (Pearson correlation coefficient ~ -0.5; Fig. 8 (vi)) and aligns with findings from previous studies, which demonstrate significant negative correlations between TC translation speed and flood severity (e.g., Hall and Kossin 2019; Gori et al. 2020; Titley et al. 2021).

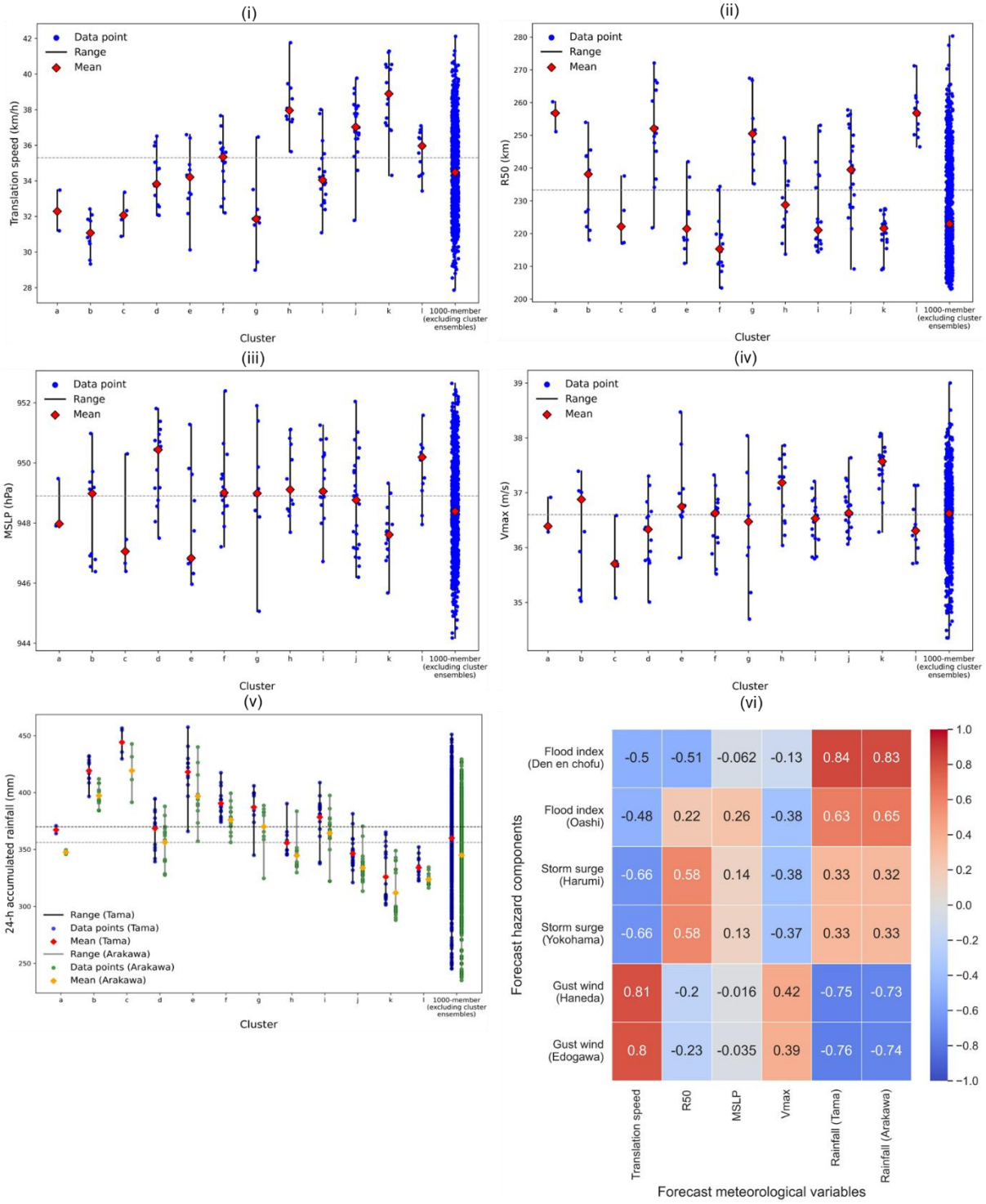

FIG. 8. Forecasted 6-h averaged (3-h before and 3-h after landfall) meteorological variables associated with Pareto optimal solutions in each cluster (Fig. 7 (a-l)): (i) translation speed; (ii) radius of 50-kt wind; (iii) mean sea level pressure; (iv) 10-minute sustained wind speed. (v) Forecasted 24-h (12 October 2023 00:00-23:00 JST) basin averaged accumulated rainfall associated with Pareto optimal solutions in each cluster (Fig. 7); (vi) Pearson correlation matrix for meteorological forecasts in panels (i-v) and MHWCS in Fig. 7 (a-l; red lines). The dotted black (panels i-v) and grey (panel v) lines represent the ensemble mean for each meteorological variable, derived from the 153 MHWCS forecasts.

While faster-moving ensembles, such as those in cluster (k), are forecasted to cause weaker flooding hazards due to the reduced duration of rainfall exposure, they are also predicted to generate the lowest storm surges in inner Tokyo Bay (Fig. 7 (k); Fig. 8 (vi)), as compared to Pareto-optimal solutions in Fig. 7(g). In addition to translation speed (S), the spread of the R_{50} (Fig. 8 (ii)) and track (Fig. 9 (g), (k)) substantially influence surge heights. Although the Pareto-optimal solutions in both clusters are forecasted to make landfall approximately 75 km west of the longitudinal axis of Tokyo Bay (Figs. 9(g) and 9(k)), their tracks exhibit distinct behaviors. Tracks in cluster (g) diverge significantly, move at a slower S (~32 km/h; Fig. 8 (i)) and maintain a larger R_{50} (~250 km; Fig. 8 (ii)) as they approach inner Tokyo Bay. With a longer duration of exposure, this large swath of strong winds directly impacts a broader sea area, inducing motion in a larger volume of water in inner Tokyo Bay (Fig. 7(g)). This phenomenon supports earlier numerical analyses that highlight the likelihood of severe storm surge scenarios in upper Tokyo Bay when a large and intense TC moves slowly and parallel to the bay's longitudinal axis after making landfall ~25 km southwest of the area (Islam and Takagi 2020a,b, 2021). Conversely, ensembles in cluster (k) exhibit faster S (~39 km/h; Fig. 8 (i)) and smaller R_{50} (~222 km; Fig. 8 (ii)), resulting in less water being pushed toward Tokyo Bay (Fig. 7(k)) compared to all other clusters in Fig. 7. Furthermore, we observed variability in the worst storm surge scenarios under similar meteorological conditions, except for differences in TC size. For example, clusters (e) and (g) share comparable S (Fig. 8 (i)), V_{max} (Fig. 8 (iv)), and trajectory forecasts (Fig. 9), yet differ significantly in their spatial strong wind footprints. However, both clusters are significantly distinct from the forecasted spatial strong wind footprints (R_{50}; Fig. 8(ii)). This distinction leads to approximately 9% variation in worst-case storm surge forecasts (Figs. 7(e) and 7(g)). This behavior is expected, as TC size is a well-established predictor of peak storm surges (Irish et al. 2008; Islam and Takagi 2020a) and aligns with the association shown in Fig. 8 (vi; Pearson correlation coefficient 0.58).

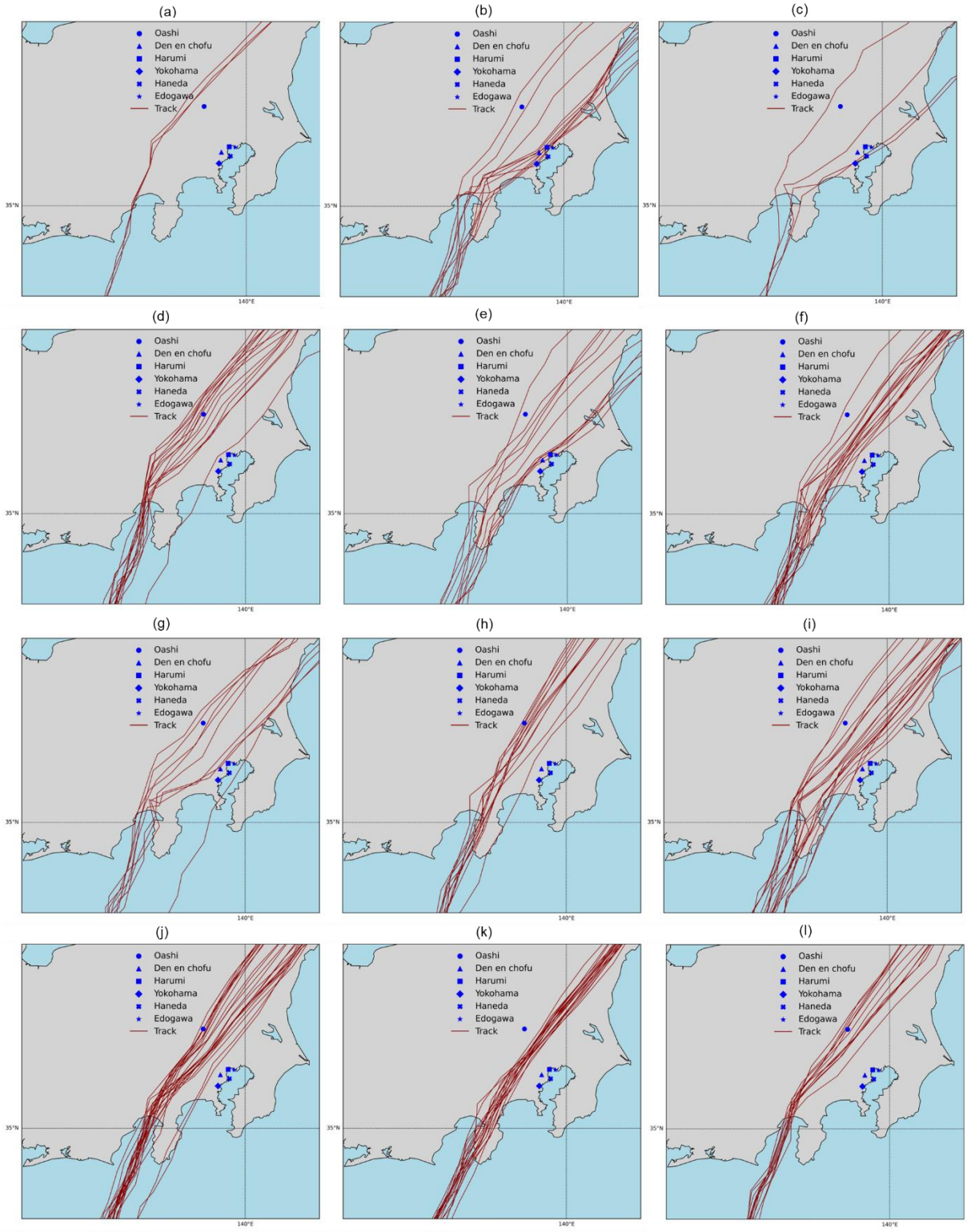

FIG. 9. Forecasted TC Hagibis tracks with a 39-h lead time corresponding to each MHWCS (Pareto-optimal solutions) identified in Fig. 7. Pannels (a-l) represent the clusters shown in Fig. 7 (a-l). Red lines indicate the forecasted TC tracks, while blue symbols denote the forecast locations considered in this study.

The analysis above demonstrates that slow-moving ensemble forecasts, when combined with other meteorological conditions, are likely to intensify flooding and storm surge hazards.

However, fast-moving forecasts cannot be overlooked as it is likely to cause strong wind hazards (Pearson correlation coefficient ~ 0.8; Fig. 8 (vi)). For instance, both cluster (h) and cluster (k) in Fig. 7 are forecasted to produce the most severe wind hazard scenarios in Tokyo, surpassing other forecasts, including clusters (a), (b), (c), and (g). Both cluster (h) and cluster (k) are associated with the fastest ensemble forecasts (~39 km/h; Fig. 8(i)), characterized by small R_{50} (~ 225 km; Fig. 8 (ii)) and intense V_{max} (~ 37 m/s; Fig. 8 (iv)). It is reasonable, as rapid forward motion combined with strong rotational winds amplifies the total wind intensity, particularly in the right-front quadrant (Olfateh et al. 2017; Klotz and Jiang 2017) where the forecast points are located (Figs. 9h and 9k). This phenomenon results in catastrophic wind damage upon landfall. Furthermore, intense storms tend to be smaller in size, consistent with findings from earlier studies (Carrasco et al. 2014; Gori et al. 2020). Conversely, ensemble forecasts in clusters (a), (b), (c), and (g) are characterized by slower S (~32 km/h; Fig. 8 (i)), larger R_{50} (~241 km; Fig. 8 (ii)), and slightly weaker V_{max} (~ 36 m/s; Fig. 8 (iv)) compared to the ensembles in clusters (h) and (k). It is also noteworthy that the tracks associated with clusters (h) and (k) maintain relatively straight trajectories before and after landfall, unlike the diverging tracks seen in other clusters (Fig. 9). These straight paths after landfall increase the likelihood of strong winds impacting the land, as they minimize interaction with land or atmospheric conditions that could weaken the TC.

Although single-hazard-based worst case scenario forecasts tend to exhibit the characteristics discussed above, no single predictor for MHWCS was identified in our ensemble forecasts. For instance, the ensemble means of S, R_{50}, $MSLP$, V_{max}, and basin averaged accumulated rainfall associated with the special cluster (i) in Fig. 7 are comparable to the total population ensemble means (Fig. 8 (i-v)). In general, the ensembles in cluster (i) exhibit moderate meteorological characteristics, representing a balanced condition that is not evident in other clusters (Fig. 8 (i-v)). In other words, the special set of Pareto-optimal solutions in Fig. 7(i), capable of producing significant multi-hazard impacts across all investigated locations, does not necessarily correspond to the most extreme meteorological conditions compared to other forecast conditions observed from a single-hazard perspective. However, the uncertainty ranges for S (Fig. 8 (i)) and R_{50} (Fig. 8 (ii)) within cluster (i) are notably wide. This spread is expected, as slow-moving (fast-moving) and large (small) TCs are individually capable of generating worst-case scenarios from a single-hazard perspective. It is also noteworthy that the tracks associated with single-hazard worst case scenarios (clusters (c), (g),

and (k) in Fig. 9) are enveloped by the ensemble forecasts of cluster (i). This indicates that the ensemble spread is sufficiently large to represent track uncertainty in MHWCS predictions.

4. Discussion and conclusions

The application of ensemble TC forecasting for predicting MHWCS has not been fully exploited, despite its widespread use in forecasting TC track, intensity, and genesis. Enhanced analytical approaches can unlock the full potential of ensemble forecasting. Here, we propose Pareto-optimality as a novel, efficient, and practical method to identify meaningful ensemble TC (Hagibis) forecasts from a large ensemble (1,000 members) to objectively assess MHWCS for a target region. The variability within the ensemble (e.g., track, intensity, size, translation speed, rainfall) across different forecast locations makes it challenging for decision makers in planning effective preparedness measures against multi-hazard risks. Our analysis demonstrates that meaningful trade-offs among competing hazard objectives can be identified by selecting Pareto-optimized forecasts. By accounting for uncertainties in ensemble multi-hazard forecasts, Pareto optimal solutions illustrate a compact view of MHWCS, maximizing multi-hazard intensities relative to the ensemble mean. Additionally, these solutions can aid emergency managers in understanding how combinations of TC meteorological variables—such as track, translation speed, size, intensity, and rainfall—contribute to shaping worst-case scenarios. Although operational implementation of MHWCS prediction for each ensemble member poses significant challenges within the current global forecasting context, our proposed multi-objective framework can extract meaningful MHWCS from large ensemble forecasts within minutes. This runtime efficiency makes it a viable option for operational hazard forecasting systems, assuming that large ensemble forecasts will become more computationally affordable and practical in the near future with the advancement of artificial intelligence-based weather forecasting (Li et al. 2024; Price et al. 2025).

The significance of evaluating ensemble forecasts has long been recognized for quantifying single-hazard worst-case scenarios (Hoffman and Gombos 2012; Scher et al. 2021; Islam et al. 2023a). Nevertheless, the application of multi-objective approaches, such as Pareto optimization, in MHWCS analysis remains noticeably underexplored. During a TC event, preparedness measures including effective evacuation planning, emergency resource allocation, and warning issuance involve multi-criteria problems such as multi-hazard intensity, population vulnerability, and available evacuation resources. Traditionally, this decision-making process has relied on the severity of the predicted single hazard (e.g., storm

surge) based worst case scenarios (Hasegawa et al. 2017; NHC 2023; Sharma et al. 2022). However, this approach does not fully capture the diversity and collective impact of individual hazard components in a target location, which can lead to ineffective decision making. While such a complex decision-making process can certainly be improved by quantifying the uncertainty in multi-hazard forecast, incorporating Pareto-optimality can further maximize the benefits of it.

In Japan, JMA is responsible for issuing TC related alerts at national level, with distinct alerts provided for each hazard component. Notably, no unified alert system exists to address combined multi-hazard risks. Furthermore, the decision to implement specific actions, such as evacuation orders, rests with local governments, which base their decisions on JMA guidelines and predefined warning criteria (e.g., reference tidal height set by local government, JMA 2023b). At first glance, it might seem sufficient for a city or local government to focus solely on single-hazard worst-case (e.g., storm surge) at their designated reference points when issuing warnings, without considering MHWCS. For example, disaster risk managers in Den-en-chofu might not perceive the need to account for storm surge impacts in Harumi. In such cases, detailed localized risk, like that presented in Fig. 4, may appear adequate. Consequently, the necessity for considering trade-offs among competing hazard components, as depicted in Fig. 7, could be questioned. However, from a multi-hazard risk perspective, we emphasize the importance of analyzing diverse trade-offs across multiple hazard components and geographic locations. The rationale for this is twofold. First, holistic multi-hazard analyses are essential for efficiently allocating resources at a national level. This includes provisions such as rescue operations, food, water, and medical supplies. Unlike single-hazard scenarios, MHWCS forecasts capture the combined impacts of hazards (e.g., storm surge, river flooding, and wind hazards), enabling more strategic resource planning to address complex disaster impacts comprehensively. Second, diversity in multi-hazard trade-off scenarios facilitates intercity cooperation before and after mega-disasters. For example, a city less affected by storm surges might be severely impacted by flooding or wind hazards, necessitating support from neighboring cities. Conversely, areas less affected by wind hazards may assist in accommodating evacuees or sharing resources in the post-disaster period. Such interdependencies highlight the need for a multi-hazard approach that considers trade-offs and synergies between hazards across regions. In this regard, MHWCS analyses expand the scope of disaster preparedness, encouraging intercity collaboration and fostering resilience beyond the scope of single-hazard frameworks. Moreover, the MHWCS approach enables risk

managers and forecasters to better understand how the interactions among meteorological variables influence worst-case scenarios. This understanding is critical for designing evacuation plans that account for multi-hazard risks, such as simultaneous storm surges and riverine flooding or the compounded impacts of wind and flooding hazards. For instance, while localized storm surge-focused planning might suffice for individual cities, MHWCS predictions highlight broader regional impacts, ensuring preparedness for cascading effects that could disrupt neighboring areas.

While ensemble forecast is certainly beneficial to analyze MHWCS, we particularly emphasize over a large ensemble forecast (e.g., 1000-member). Unlike the small number of ensemble forecast (e.g., operational 20-member JMA ensemble forecast (MEPS)), large ensemble forecast can reduce sampling error (Kobayashi et al. 2020; Duc et al. 2021) by providing a broader range of possible outcomes for TCs, capturing variations in meteorological parameters. This comprehensive representation of uncertainty is crucial for MHWCS, as each hazard component (e.g., storm surge, river flooding, gust wind) can respond differently to these variables. Moreover, larger ensembles allow for the identification of diverse Pareto-optimal solutions, offering a more detailed exploration of trade-offs among competing hazard objectives. This diversity ensures that MHWCS analyses account for complex interdependencies between hazards, which may be missed in smaller ensembles and increases the probability of identifying extreme yet plausible MHWCS.

Finally, the present study highlights the efficacy of applying Pareto-optimality in extracting MHWCS from an ensemble forecast, however, it relies on specific numerical and statistical models and assumptions that may not fully capture all potential uncertainties, such as those related to model physics. Additionally, the analysis is focused on a single TC (Hagibis) and a specific geographic region, limiting the generalizability of the findings to other regions or TC events. Future research should explore the application of this framework to other regions and hazard contexts and incorporate additional sources of uncertainty.

Acknowledgement

The authors declare no conflicts of interest relevant to this study. This work is supported by JST Moonshot R&D project (Grant Number: JPMJMS2281), the Program for Promoting Research on the Supercomputer Fugaku JPMXP1020351142 “Large Ensemble Atmospheric and Environmental Prediction for Disaster Prevention and Mitigation” (hp210166), JSPS

Grant-in-Aid for Early Career Scientists (Grant Number: 23K13531), JSPS KAKENHI (Grant Number: 22K20455), and The Obayashi Foundation Research Grant.

Data availability statement

Observed river water level, storm surge, and gust wind data can be downloaded from MLIT (2024), JMA (2022), and JMA (2024), respectively. TC best track data can be derived from JMA (2021). Ensemble TC track forecast data analyzed in this study is provided in Islam et al. (2023c). All results were analyzed by using Jupyter Notebook 6.5.4 and visualized by using matplotlib 3.7.1, ArcMap 10.8, and Panoply 4.12.13.

References

Alipour, A., F. Yarveysi, H. Moftakhari, J. Y. Song, and H. Moradkhani, 2022: A Multivariate Scaling System Is Essential to Characterize the Tropical Cyclones' Risk. *Earth's Future*, **10**, e2021EF002635, https://doi.org/10.1029/2021EF002635.

Carrasco, C. A., C. W. Landsea, and Y.-L. Lin, 2014: The Influence of Tropical Cyclone Size on Its Intensification. https://doi.org/10.1175/WAF-D-13-00092.1.

Das, S., A. Jessica, M. Ishiwatari, T. Komino, and R. Shaw, 2020: *Lessons from Hagibis: Learning to Cope with Intensifying Disasters in the Age of New Normal*. CWS Japan, https://jcc-drr.net/wpJD/wp-content/uploads/2020/03/HagibisOnePageScroll_final.pdf.

Dilley, M., R. S. Chen, U. Deichmann, A. L. Lerner-Lam, and M. Arnold, 2005: *Natural Disaster Hotspots: A Global Risk Analysis*. Washington, DC: World Bank,.

Du, H., K. Fei, and L. Gao, 2024: Nonlinear Tide-River-Surge Interactions and Their Impacts on Compound Flooding During Typhoon Hato in the Pearl River Delta. *Journal of Geophysical Research: Oceans*, **129**, e2023JC020673, https://doi.org/10.1029/2023JC020673.

Duc, L., T. Kawabata, K. Saito, and T. Oizumi, 2021: Forecasts of the July 2020 Kyushu Heavy Rain Using a 1000-Member Ensemble Kalman Filter. *Sola*, **17**, 41–47, https://doi.org/10.2151/sola.2021-007.

Frey, B. J., and D. Dueck, 2007: Clustering by Passing Messages Between Data Points. *Science*, **315**, 972–976, https://doi.org/10.1126/science.1136800.

Gombos, D., and R. N. Hoffman, 2013: Ensemble-Based Exigent Analysis. Part I: Estimating Worst-Case Weather-Related Forecast Damage Scenarios. https://doi.org/10.1175/WAF-D-12-00080.1.

Gori, A., N. Lin, and D. Xi, 2020: Tropical Cyclone Compound Flood Hazard Assessment: From Investigating Drivers to Quantifying Extreme Water Levels. *Earth's Future*, **8**, e2020EF001660, https://doi.org/10.1029/2020EF001660.

Greenslade, D., and Coauthors, 2017: An operational coastal sea level forecasting system. *Australasian Coasts & Ports 2017: Working with Nature*, 514–520.

Hall, T. M., and J. P. Kossin, 2019: Hurricane stalling along the North American coast and implications for rainfall. *npj Climate and Atmospheric Science*, **2**, 1–9, https://doi.org/10.1038/s41612-019-0074-8.

Hasegawa, H., N. Kohno, M. Higaki, and M. Itoh, 2017: *Upgrade of JMA's Storm Surge Prediction for the WMO Storm Surge Watch Scheme (SSWS)*. RSMC Tokyo - Typhoon Center, https://www.jma.go.jp/jma/jma-eng/jma-center/rsmc-hp-pub-eg/techrev/text19-2.pdf.

Hoffman, R. N., and D. Gombos, 2012: Hurricane Irene (2011) "worst-case" estimates of wind damage to property from exigent analysis of ECMWF ensemble forecasts. *Geophysical Research Letters*, **39**, https://doi.org/10.1029/2012GL052646.

Irish, J. L., D. T. Resio, and J. J. Ratcliff, 2008: The influence of storm size on hurricane surge. *Journal of Physical Oceanography*, **38**, 2003–2013, https://doi.org/10.1175/2008JPO3727.1.

Ishihara, Y., and S. Kobatake, 1979: Runoff Model for Flood Forecasting. *Bulletin of the Disaster Prevention Research Institute*, **29**, 27–43.

Islam, M. R., and H. Takagi, 2020a: Typhoon parameter sensitivity of storm surge in the semi-enclosed Tokyo Bay. *Frontiers of Earth Science*, **14**, 553–567, https://doi.org/10.1007/s11707-020-0817-1.

——, and ——, 2020b: On the Importance of Typhoon Size in Storm Surge Forecasting. *Water, Flood Management and Water Security Under a Changing Climate: Proceedings from the 7th International Conference on Water and Flood Management*, A. Haque and A.I.A. Chowdhury, Eds., Springer International Publishing, 153–162.

——, and ——, 2021: Statistical significance of tropical cyclone forward speed on storm surge generation: retrospective analysis of best track and tidal data in Japan. *Georisk: Assessment and Management of Risk for Engineered Systems and Geohazards*, **15**, 247–257, https://doi.org/10.1080/17499518.2020.1756345.

——, C.-Y. Lee, K. T. Mandli, and H. Takagi, 2021: A new tropical cyclone surge index incorporating the effects of coastal geometry, bathymetry and storm information. *Sci Rep*, **11**, 16747, https://doi.org/10.1038/s41598-021-95825-7.

——, M. Satoh, and H. Takagi, 2022: Tropical Cyclones Affecting Japan Central Coast and Changing Storm Surge Hazard since 1980. *Journal of the Meteorological Society of Japan. Ser. II*, **100**, 493–507, https://doi.org/10.2151/jmsj.2022-024.

——, L. Duc, and Y. Sawada, 2023a: Assessing Storm Surge Multiscenarios Based on Ensemble Tropical Cyclone Forecasting. *Journal of Geophysical Research: Atmospheres*, **128**, e2023JD038903, https://doi.org/10.1029/2023JD038903.

——, ——, ——, and M. Satoh, 2023b: Does mean sea level trend mask historical storm surge trend: evidence from tropical cyclones affecting Japan since 1980. *Environ. Res. Lett.*, **18**, 085004, https://doi.org/10.1088/1748-9326/ace985.

Islam, Md. R., L. Duc, and Y. Sawada, 2023c: Dataset for "Assessing Storm Surge Multi-Scenarios based on Ensemble Tropical Cyclone Forecasting" paper. https://doi.org/10.5281/zenodo.8275484.

Japan Oceanographic Data Center, 2020: 500m Gridded Bathymetry Data. https://www.jodc.go.jp/jodcweb/JDOSS/infoJEGG.html (Accessed January 8, 2021).

JMA, 2021: Japan Meteorological Agency | RSMC Tokyo - Typhoon Center | Best Track Data [Dataset]. https://www.jma.go.jp/jma/jma-eng/jma-center/rsmc-hp-pub-eg/trackarchives.html (Accessed March 13, 2021).

——, 2022: Tidal observation data [Dataset]. https://www.data.jma.go.jp/gmd/kaiyou/db/tide/genbo/index.php (Accessed June 30, 2022).

——, 2023a: Japan Meteorological Agency｜Numerical Weather Prediction Activities. https://www.jma.go.jp/jma/en/Activities/nwp.html (Accessed March 10, 2023).

——, 2023b: Weather warnings/advisories. https://www.jma.go.jp/jma/kishou/know/bosai/warning.html (Accessed August 8, 2023).

——, 2024: JMA past weather data. http://www.data.jma.go.jp/obd/stats/etrn/index.php (Accessed May 12, 2021).

——, n.d: Wind force scale. https://www.data.jma.go.jp/multi/cyclone/cyclone_wind_advisory.html?lang=en (Accessed December 3, 2024).

Klotz, B. W., and H. Jiang, 2017: Examination of Surface Wind Asymmetries in Tropical Cyclones. Part I: General Structure and Wind Shear Impacts. https://doi.org/10.1175/MWR-D-17-0019.1.

Kobayashi, K., L. Duc, Apip, T. Oizumi, and K. Saito, 2020: Ensemble flood simulation for a small dam catchment in Japan using nonhydrostatic model rainfalls – Part 2: Flood forecasting using 1600-member 4D-EnVar-predicted rainfalls. *Natural Hazards and Earth System Sciences*, **20**, 755–770, https://doi.org/10.5194/nhess-20-755-2020.

Leonard, M., and Coauthors, 2014: A compound event framework for understanding extreme impacts. *WIREs Climate Change*, **5**, 113–128, https://doi.org/10.1002/wcc.252.

Letson, D., D. S. Sutter, and J. K. Lazo, 2007: Economic Value of Hurricane Forecasts: An Overview and Research Needs. *Natural Hazards Review*, **8**, 78–86, https://doi.org/10.1061/(ASCE)1527-6988(2007)8:3(78).

Li, L., R. Carver, I. Lopez-Gomez, F. Sha, and J. Anderson, 2024: Generative emulation of weather forecast ensembles with diffusion models. *Science Advances*, **10**, eadk4489, https://doi.org/10.1126/sciadv.adk4489.

Liu, C., Q. Xiao, and B. Wang, 2008: An Ensemble-Based Four-Dimensional Variational Data Assimilation Scheme. Part I: Technical Formulation and Preliminary Test. https://doi.org/10.1175/2008MWR2312.1.

Ma, W., and Coauthors, 2021: Applicability of a nationwide flood forecasting system for Typhoon Hagibis 2019. *Sci Rep*, **11**, 10213, https://doi.org/10.1038/s41598-021-89522-8.

Messmer, M., and I. Simmonds, 2021: Global analysis of cyclone-induced compound precipitation and wind extreme events. *Weather and Climate Extremes*, **32**, 100324, https://doi.org/10.1016/j.wace.2021.100324.

MLIT, 2024: Water Information System. http://www1.river.go.jp/ (Accessed November 29, 2024).

Molina, R., and I. Rudik, 2024: The Social Value of Hurricane Forecasts. https://doi.org/10.3386/w32548.

Nagata, K., 2011: *Quantitative precipitation estimation and quantitative precipitation forecasting by the Japan Meteorological Agency.* RSMC Tokyo–Typhoon Center Technical Review, https://www.jma.go.jp/jma/jma-eng/jma-center/rsmc-hp-pub-eg/techrev/text13-2.pdf.

NHC, 2023: Sea, Lake, and Overland Surges from Hurricanes (SLOSH). https://www.nhc.noaa.gov/surge/slosh.php (Accessed January 19, 2023).

Oizumi, T., K. Saito, J. Ito, T. Kuroda, and L. Duc, 2018: Ultra-High-Resolution Numerical Weather Prediction with a Large Domain Using the K Computer: A Case Study of the Izu Oshima Heavy Rainfall Event on October 15-16, 2013. *Journal of the Meteorological Society of Japan. Ser. II*, **96**, 25–54, https://doi.org/10.2151/jmsj.2018-006.

——, ——, L. Duc, and J. Ito, 2020: Ultra-high Resolution Numerical Weather Prediction with a Large Domain Using the K Computer. Part 2: The Case of the Hiroshima Heavy Rainfall Event on August 2014 and Dependency of Simulated Convective Cells on Model Resolutions. *Journal of the Meteorological Society of Japan. Ser. II*, **98**, 1163–1182, https://doi.org/10.2151/jmsj.2020-060.

Olfateh, M., D. P. Callaghan, P. Nielsen, and T. E. Baldock, 2017: Tropical cyclone wind field asymmetry—Development and evaluation of a new parametric model. *Journal of Geophysical Research: Oceans*, **122**, 458–469, https://doi.org/10.1002/2016JC012237.

Ono, K., M. Kunii, and Y. Honda, 2021: The regional model-based Mesoscale Ensemble Prediction System, MEPS, at the Japan Meteorological Agency. *Quarterly Journal of the Royal Meteorological Society*, **147**, 465–484, https://doi.org/10.1002/qj.3928.

Ota, T., 2017: *New index for heavy rainfall and flood warning*. Japan Meteorological Agency, https://www.jma.go.jp/jma/kishou/books/yohkens/22/chapter2.pdf (Accessed November 29, 2024).

——, and Y. Makihara, 2018: Technical developments for mitigating disasters from Inundation and flood and dissemination of their results. *Tenki*.

——, and Coauthors, 2023: JMA's hazard potential index and real-time risk map related to heavy rain. *Weather service bulletin*, **90**, 1–96.

Price, I., and Coauthors, 2025: Probabilistic weather forecasting with machine learning. *Nature*, **637**, 84–90, https://doi.org/10.1038/s41586-024-08252-9.

Sadegh, M., H. Moftakhari, H. V. Gupta, E. Ragno, O. Mazdiyasni, B. Sanders, R. Matthew, and A. AghaKouchak, 2018: Multihazard Scenarios for Analysis of Compound Extreme Events. *Geophysical Research Letters*, **45**, 5470–5480, https://doi.org/10.1029/2018GL077317.

Saito, K., and Coauthors, 2006: The Operational JMA Nonhydrostatic Mesoscale Model. *Monthly Weather Review*, **134**, 1266–1298, https://doi.org/10.1175/MWR3120.1.

Scher, S., S. Jewson, and G. Messori, 2021: Robust Worst-Case Scenarios from Ensemble Forecasts. https://doi.org/10.1175/WAF-D-20-0219.1.

Sharma, M., and Coauthors, 2022: *Forecasting Tropical Cyclone Hazards and Impacts*. 10th International Workshop on Tropical Cyclones (IWTC-10), https://community.wmo.int/en/iwtc-10-reports (Accessed January 16, 2023).

Shimozono, T., Y. Tajima, K. Kumagai, T. Arikawa, Y. Oda, Y. Shigihara, N. Mori, and T. Suzuki, 2020: Coastal impacts of super typhoon Hagibis on Greater Tokyo and Shizuoka areas, Japan. *Coastal Engineering Journal*, **62**, 129–145, https://doi.org/10.1080/21664250.2020.1744212.

Swinbank, R., and Coauthors, 2016: The TIGGE Project and Its Achievements. *Bulletin of the American Meteorological Society*, **97**, 49–67, https://doi.org/10.1175/BAMS-D-13-00191.1.

Tanaka, N., T. Ota, and Y. Makihara, 2008: Flood warning/advisory improvement based on JMA Runoff Index. *Weather service bulletin*, **75**, 35–50.

Titley, H. A., M. Yamaguchi, and L. Magnusson, 2019: Current and potential use of ensemble forecasts in operational TC forecasting: results from a global forecaster survey. *Tropical Cyclone Research and Review*, **8**, 166–180, https://doi.org/10.1016/j.tcrr.2019.10.005.

——, H. L. Cloke, S. Harrigan, F. Pappenberger, C. Prudhomme, J. C. Robbins, E. M. Stephens, and E. Zsótér, 2021: Key Factors Influencing the Severity of Fluvial Flood Hazard from Tropical Cyclones. https://doi.org/10.1175/JHM-D-20-0250.1.

Valle-Levinson, A., M. Olabarrieta, and L. Heilman, 2020: Compound flooding in Houston-Galveston Bay during Hurricane Harvey. *Science of The Total Environment*, **747**, 141272, https://doi.org/10.1016/j.scitotenv.2020.141272.

Wahl, T., S. Jain, J. Bender, S. D. Meyers, and M. E. Luther, 2015: Increasing risk of compound flooding from storm surge and rainfall for major US cities. *Nature Clim Change*, **5**, 1093–1097, https://doi.org/10.1038/nclimate2736.